Sensors and Materials, Vol. 36, No. 6 (2024) 2225–2235
MYU Tokyo

S & M 3664

Point-of-Care Immunosensor for Epstein–Barr Virus Infection Detection Using a Biocarbon-based Platform

Chen Chen and Meiling Liu*

Otolaryngology Department, The First Hospital of China Medical University, Shenyang, China

(Received March 4, 2024; accepted May 27, 2024)

Keywords: flavivirus, neuroinflammation, electrochemical impedance, nanomaterials, infection control

We present the development of a novel point-of-care electrochemical immunosensor for the detection of the Epstein–Barr virus capsid antigen (EBVCA-IgA) using a biocarbon-modified screen-printed electrode platform. The biosensor achieves sensitive and rapid detection within a broad linear range of 0.1 pM to 10 nM of EBVCA-IgA, with an impressive limit of detection of 33 fM. The key to its practical utility is that the sensor operates efficiently, providing results in under one hour, which is a significant improvement over traditional methods such as enzyme-linked immunosorbent assays and polymerase chain reaction that typically exceed two hours. We also emphasize the sensor's high selectivity by demonstrating minimal cross-reactivity with other common respiratory viruses. With its combination of rapidity, sensitivity, and simplicity, this biosensor represents a significant advancement in Epstein–Barr virus (EBA) diagnostics, which makes it particularly beneficial in clinical and low-resource settings where rapid and reliable testing is paramount.

1. Introduction

Epstein–Barr virus (EBV) is one of the most common human viruses, infecting more than 90% of the world's adult population. Primary infection with EBV usually occurs during childhood and causes no symptoms or only mild cold-like symptoms.[1,2] However, EBV infection later in life can lead to infectious mononucleosis with symptoms including fever, sore throat, swollen lymph nodes, and fatigue.[3] Although EBV infection is often asymptomatic after the acute phase, the virus persists lifelong in a latent state in B cell reservoirs.[4] Periodic reactivation can occur, whereby an infectious virus can be shed in saliva. EBV infection has been associated with certain types of cancers including Burkitt's lymphoma, nasopharyngeal carcinoma, and Hodgkin's disease.[5]

The diagnosis of acute EBV infection involves testing for the presence of the EBV capsid antigen (EBVCA-IgA) that appear early during primary infection.[6] The most common methods for EBV antibody detection are enzyme-linked immunosorbent assay (ELISA) and indirect immunofluorescence assay, which require trained personnel, long analysis times of more than two hours, and specialized laboratory infrastructure.[7] Although sensitive and reliable, these

*Corresponding author: e-mail: 13904037545@163.com
https://doi.org/10.18494/SAM5015

ISSN 0914-4935

conventional EBV diagnostic methods pose limitations for rapid clinical decision making and point-of-care testing.[8]

Recent advances in biosensor technology have resulted in the development of rapid, portable devices that enable the real-time analysis of clinically relevant biomarkers.[9] In particular, electrochemical biosensors have shown substantial promise for point-of-care testing applications owing to their simple instrumentation, ease of miniaturization, and compatibility with microfabrication technologies.[10] Electrochemical immunosensors using antibodies as biorecognition elements have been used for detecting viruses, bacteria, proteins, small molecules, and more.[11–15] Screen-printed electrodes and various nanomaterial-modified electrode substrates have been utilized as platforms for the sensitive electrochemical biosensing of analytes. Although there have been some reports on electrochemical EBV sensors based on surface plasmon resonance and potentiometry,[16,17] an immunosensor for EBV using a biocompatible carbon electrode has not yet been realized. A screen-printed electrode has emerged as a promising electrode for electrochemical biosensing owing to its attractive properties including wide potential window, low background current, chemical inertness, and amenability to surface functionalization.[18] In particular, biochar modification offers sustainability advantages along with inherent porosity and surface oxidation that can enhance biomolecule immobilization.[19] While biochar-based electrodes have been recently explored for electrochemical applications such as supercapacitors and batteries,[20,21] their potential for electrochemical sensing remains relatively untapped. The few reported biochar electrochemical sensors have demonstrated encouraging results for pesticide and heavy metal detection.[22,23] Building upon this, we sought to investigate a biochar-based screen-printed electrode as an electrochemical sensing platform for viral immunosensing. The choice of biochar aligns with the drive towards green, renewable biosensor components without compromising on analytical performance.

Here, we report the development of an ultrasensitive impedimetric immunosensor for the detection of EBVCA-IgA using a screen-printed electrode platform. The immunosensing interface relies on the covalent immobilization of the EBV antigen onto the activated carboxylated electrode surface. The subsequent binding of EBV-specific antibodies is detected by electrochemical impedance spectroscopy measurements using a redox probe in solution. We demonstrate a linear detection range from 0.1 pM to 10 nM along with a limit of detection better than those of existing EBVCA-IgA assays. The biocarbon immunosensor enables selective and reproducible EBV antibody detection within minutes using microliter sample volumes. This approach could enable the realization of inexpensive and portable devices for rapid EBV diagnosis at the point of care with utility in clinical settings and resource-limited environments.

2. Data, Materials, and Methods

2.1 Immunosensor fabrication

Biochar-modified screen-printed electrodes [BSPEs, inset of Fig. 1(a)] were used as the transducer platform for EBVCA-IgA immunosensing. The cleaned BSPE surface was then electrochemically activated by scanning the potential vs a Ag/AgCl reference electrode in 0.1 M H_2SO_4 solution to introduce carboxyl and hydroxyl groups.

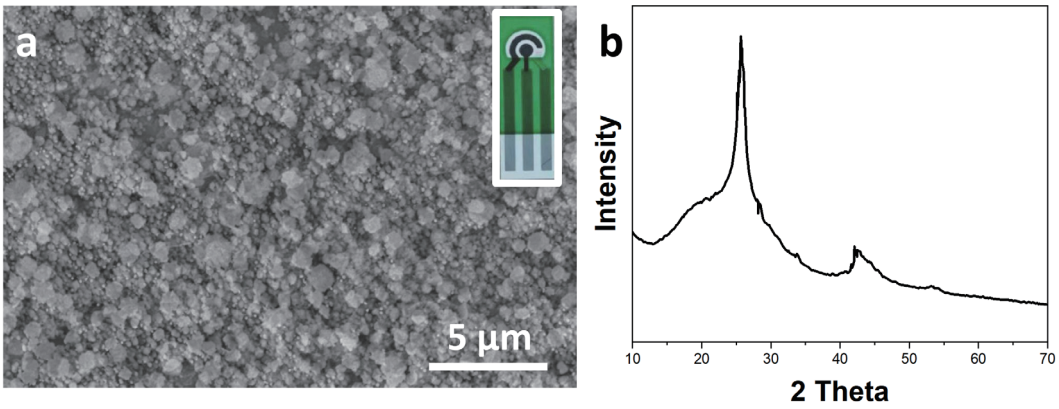

Fig. 1. (Color online) (a) SEM image and (b) XRD pattern of BSPE. Inset of (a): digital photo of BSPE.

The EBV-specific capture biomolecule immobilized onto a BSPE was a recombinant EBVCA (MyBioSource Inc.) consisting of the p18 peptide. The covalent linking of virus capsid antigens (VCAs) was achieved using 1-ethyl-3-(3-dimethylaminopropyl)carbodiimide hydrochloride/*N*-hydroxysuccinimide (EDC/NHS) coupling chemistry targeting the activated carboxyl groups on the BSPE surface. The BSPE was incubated with 5 mM EDC and 10 mM NHS prepared in 0.1 M 2-(*N*-morpholino)ethanesulfonic acid buffer (pH 5.0) for 1 h at room temperature to form reactive NHS-ester intermediates. After rinsing, the EDC/NHS-activated electrodes were treated with a 10 µg/mL VCA antigen solution diluted in PBS (pH 7.4) for 2 h under constant shaking motion at 4 °C for covalent binding. The electrodes were then rinsed gently and incubated with a 1% bovine serum albumin (BSA) solution for 30 min to block any remaining activated sites against nonspecific adsorption during subsequent immunosensing.

2.2 EBVCA-IgA sensing

The serum samples from adult donors were provided by the The First Hospital of China Medical University, and the informed consent for use of the human serum was obtained. All sample preparations were approved by the Institutional Review Committee of the relevant hospital and carried out in accordance with institutional guidelines and conformed to the relevant regulatory standards Ethical. For EBV immunosensing experiments, the EBVCA-IgA stock was spiked into 50% normal human serum to simulate clinical blood samples. The serum matrix was diluted to minimize any confounding effects in electrochemical testing.

All electrochemical tests were performed using a Metrohm Autolab potentiostat interfaced to a standard three-electrode cell comprising the EBV antigen-modified BSPE electrode as the working electrode, a Ag/AgCl reference electrode, and a platinum wire counter electrode. Cyclic voltammetry (CV) scans were recorded in a deaerated 5 mM $Fe(CN)_6^{3-/4-}$ redox probe prepared in 0.1 M PBS (pH 7.0) at a scan rate of 50 mV/s. For EBVCA-IgA immunosensing experiments, electrochemical impedance spectroscopy (EIS) served as the signal transduction method using the same $Fe(CN)_6^{3-/4-}$ redox couple. Impedance measurements were taken over a frequency

interval from 0.1 Hz to 100 kHz under open-circuit conditions with an AC voltage amplitude of 10 mV. The limit of detection (LOD) of the BSPE immunosensor was calculated from the widely accepted signal-to-noise ratio (*S*/*N*) of 3. This method defines the LOD as the analyte concentration that produces a signal three times higher than the standard deviation of the blank (noise) measurements.

The EBVCA-IgA immunosensor calibration profile was constructed by recording impedance values after incubating the VCA-modified electrodes in logarithmically diluted EBVCA-IgA serum samples for 1 h at 37 °C with gentle shaking. After each sample exposure, the electrodes were gently rinsed and EIS measurements were acquired. The relative change in charge transfer resistance (*Rct*) was calculated and correlated to the EBVCA-IgA concentration. Key analytical performance metrics including dynamic range, LOD, reproducibility, and selectivity against common interfering species were investigated. LOD was determined experimentally as the lowest EBVCA-IgA concentration distinguishable from the blank giving a relative *Rct* shift of at least three standard deviations. Four independently fabricated immunosensor chips were evaluated to validate the precision and reproducibility of the assay protocol. Selectivity testing was conducted by exposing parallel electrodes to diluted solutions of potentially cross-reactive viruses including lysozyme, thrombin, glucose oxidase, and hemoglobin.

3. Results and Discussion

3.1 Immunosensor characterizations

The morphology and microstructure of the BSPE material were investigated using SEM and X-ray diffraction (XRD) analysis. As shown in Fig. 1(a), the BSPE exhibits a rod shape surface morphology. This rod shape is characteristic of biochar materials and arises from the carbonization of biomass precursors.[24] The XRD pattern of the BSPE [Fig. 1(b)] reveals two broad diffraction peaks centered at approximately 24 and 44°, which can be assigned to the (002) and (100) planes of turbostratic carbon, respectively.[25] The absence of sharp peaks indicates the predominantly amorphous nature of the biochar with limited long-range crystalline order. This disordered structure is typical of biomass-derived carbons and offers high electrochemical reactivity.[26]

The successive immobilization of the EBV capture antigen and blocking agent onto the BSPE surface was verified by electrochemical characterization after each fabrication step. CV and EIS were performed in a 5 mM $Fe(CN)_6^{3-/4-}$ redox probe to examine the interfacial electron transfer kinetics that are highly sensitive to surface-confined layers. As shown in the CV curves (Fig. 2), the bare BSPE exhibits a typical reversible redox peak profile for the $Fe(CN)_6^{3-/4-}$ couple with defined anodic and cathodic peaks. The peak current response is a result of the rapid electron transfer kinetics at the electrode/electrolyte interface. Upon modification with the EDC/NHS-activated carboxyl groups, the CV redox peaks were slightly suppressed owing to the introduced surface functionalities that partially obstruct the interfacial electron transfer.[27] After the immobilization of the EBVCA, the redox peak current further decreased owing to the insulating protein layer on the electrode surface. Notably, the subsequent BSA blocking yielded a

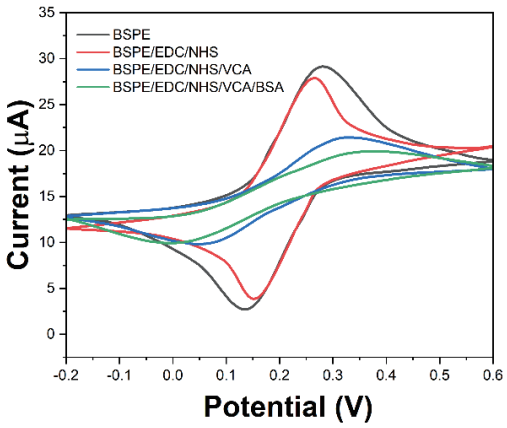

Fig. 2. (Color online) CV profiles recorded after each modification step of BSPE with EDC/NHS, EBVCA, and BSA blocking.

significant loss in the CV peak current signal, approaching a fully capacitive charging behavior.[28] This suggests a hindered access of the $Fe(CN)_6^{3-/4-}$ redox species to the underlying electrode surface owing to nonconducting, nonspecific protein blocking. The systematic decrease observed in the CV peak currents confirms a successful stepwise assembly of the immunosensor interface. Note that the $Fe(CN_6)^{3-/4-}$ redox couple is widely used in electrochemical biosensing applications owing to its favorable electron transfer kinetics and stability. In our work, the $Fe(CN_6)^{3-/4-}$ probe was used exclusively for the electrochemical characterization of the immunosensor interface and was not present during the actual virus incubation step. The EBVCA-IgA samples were diluted in a neutral pH buffer without any $Fe(CN_6)^{3-/4-}$ present, ensuring that the redox probe did not come into direct contact with the virus particles. Furthermore, we conducted additional control experiments to assess the potential impact of $Fe(CN_6)^{3-/4-}$ on the EBVCA-IgA detection. We prepared two sets of immunosensors: one following the standard protocol and the other with the inclusion of 5 mM $Fe(CN_6)^{3-/4-}$ in the incubation buffer. The EIS measurements revealed no significant difference in sensor response between the two conditions ($p > 0.05$, $n = 3$), indicating that the presence of the redox probe did not interfere with the specific binding of EBVCA-IgA to the immobilized antigens.

Complementary EIS measurements provide further in-depth quantification of the interfacial resistance changes. As depicted in the Nyquist spectra [Fig. 3(a)], *Rct* systematically increased after each surface modification, indicating impeded electron transfer kinetics.[29] Fitting the EIS data to the Randles circuit model [Fig. 3(b)] allowed the extraction of numerical *Rct* values, tabulated in Fig. 3(c). The *Rct* values were extracted by fitting the experimental EIS data to the Randles equivalent circuit model shown in Fig. 3(b). This model consists of the solution resistance (*Rs*), *Rct*, and the double layer capacitance. By applying a complex nonlinear least squares fitting algorithm to the Nyquist plots, *Rct* escalated from 17.12 Ω for the bare BSPE to 50.23 Ω after BSA blocking—an almost threefold increase. This accentuated change in interfacial electron transfer resistance with EBV immunosensing layer formation agrees with the results of CV experiments. The EIS results confirm successful biofunctionalization and appropriate blocking to yield an optimized immunosensor interface.

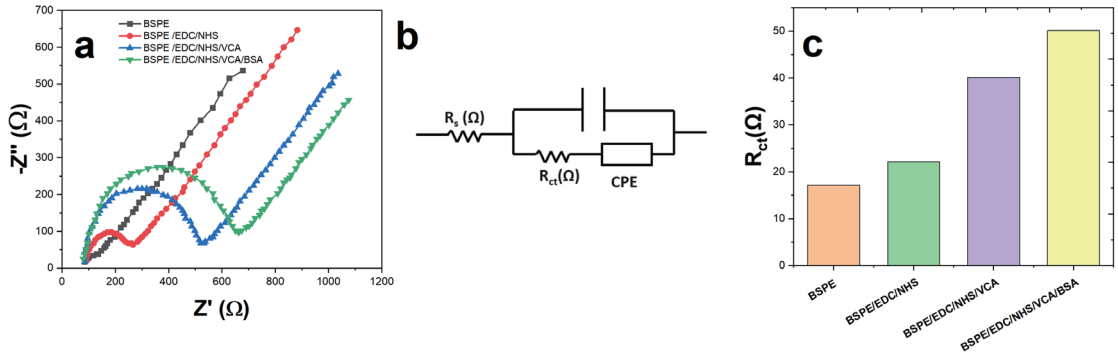

Fig. 3. (Color online) EIS characterization after each fabrication step. (a) Nyquist plots; (b) equivalent Randles circuit model used for data fitting to extract Rct values; and (c) bar chart showing gradual increase in Rct after each sequential surface modification.

Figure 4 shows the scheme of the stepwise fabrication and sensing process. First, the carboxylated BSPE is activated by incubation in an EDC/NHS solution, forming reactive NHS esters. Subsequently, the electrode is exposed to the EBVCA solution, allowing the covalent attachment of the antigens via amide bond formation with their primary amine groups. After antigen immobilization, the remaining active sites on the BSPE surface are blocked with BSA to minimize nonspecific adsorption during sensing. The functionalized immunosensor is then ready for EBV antibody detection. When the sensor is incubated with a sample containing EBV antibodies, specific binding occurs between the antibodies and the immobilized antigens. This immunocomplex formation on the electrode surface hinders the electron transfer of the $Fe(CN)_6^{3-/4-}$ redox probe, leading to an increase in *Rct*. The magnitude of the *Rct* change, measured by EIS, is proportional to the concentration of EBV antibodies in the sample, enabling quantitative detection.

3.2 Immunosensor optimizations

The immobilization of EBV capture antigens onto the BSPE surface is a critical step that determines the immunosensor sensitivity. Two key parameters that were optimized were the EDC/NHS activation time and the VCA antigen concentration. EDC/NHS reactions were performed by incubating the BSPE in 5 mM EDC + 10 mM NHS prepared in 0.1 M MES buffer (pH 5.0) for various durations in the range of 30–120 min. After immobilizing a constant 50 µg/mL VCA antigen concentration, the resulting immunosensor response was characterized by EIS. As depicted in Fig. 5(a), the *Rct* change increased gradually after 10 min to 60 min of activation owing to the higher extent of EDC/NHS ester groups available for covalent coupling. However, only a marginal improvement in Δ*Rct* was observed between 60 and 120 min activation durations. Thus, the intermediate 60 min activation time was chosen for the optimal balance between antigen loading and process efficiency.

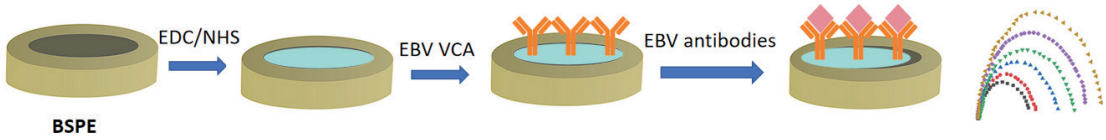

Fig. 4. (Color online) Scheme of the stepwise fabrication of immunosensor and sensing process.

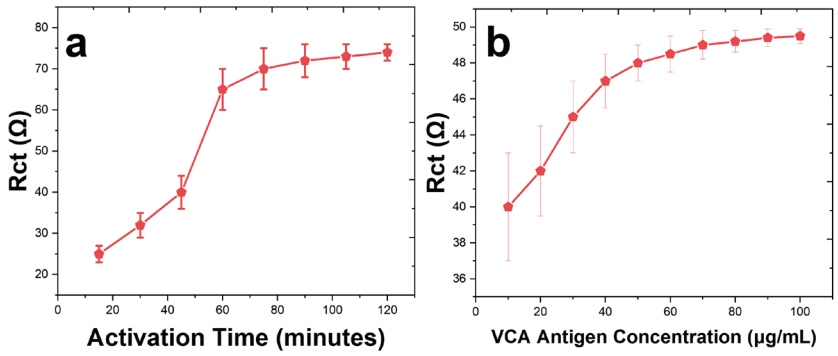

Fig. 5. (Color online) Optimization of (a) EDC/NHS activation duration and (b) VCA antigen concentration for EBVCA-IgA immunosensing at BSPE.

Next, the VCA antigen concentration from 10 to 100 μg/mL prepared in PBS (pH 7.4) applied for immobilization onto the activated BSPE was investigated. As displayed in Fig. 5(b), elevating the antigen concentration progressively increased the immunosensor response judged on the basis of *Rct* changes. This correlates to the higher antigen loading enabling improved virus capture. However, beyond 50 μg/mL, the enhancement tapered off, indicating that a saturation coverage on the electrode was attained. Excessively high antigen concentrations risk multilayer deposition that could impede electron transfer. Therefore, an intermediate 50 μg/mL VCA concentration was selected for optimal immunosensor performance. The optimized 60 min EDC/NHS activation coupled with 50 μg/mL VCA antigen immobilization was implemented for the fabrication of BGCE-based EBV immunosensing interfaces in subsequent studies.

3.3 Analytical performance

The BGCE-based EBVCA-IgA immunosensor was calibrated using standardized EBVCA-IgA spiked into 50% normal human serum. After incubating the electrodes in progressively higher virus concentrations and recording the EIS responses, a calibration plot was constructed correlating the *Rct* changes to the EBVCA-IgA concentration. As displayed in Fig. 6(a), the immunosensor exhibits a broad linear dynamic range spanning 0.1 pM to 10 nM with a linear regression coefficient of 0.998. This wide quantitative detection range covers clinically relevant viral loads in patient blood/serum samples during EBV infection. A LOD of 33 fM EBVCA-IgA was derived, which is adequate for diagnosing acute infection phases.

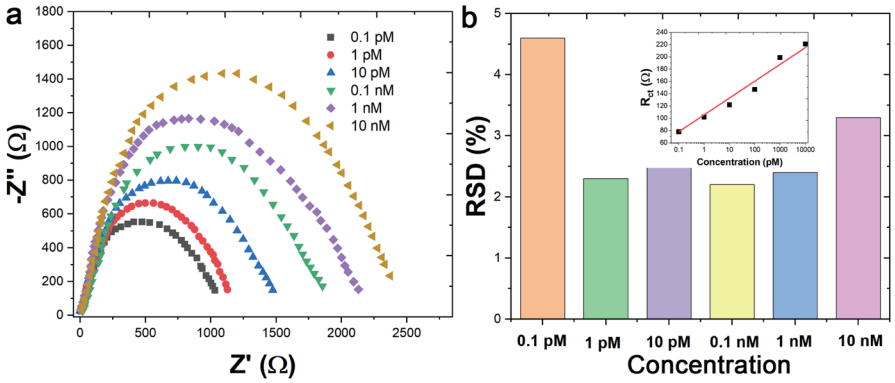

Fig. 6. (Color online) (a) EIS profile of BSPE immunosensor with spiked EBVCA-IgA concentration in serum over a 0.1 pM to 10 nM range. (b) Repeatability of the EBVCA-IgA immunosensor expressed as RSD among four independently prepared electrodes. Inset of (b): plots of EBVCA-IgA concentration vs *Rct*.

The reproducibility of the optimized EBVCA-IgA immunosensing protocol was investigated by comparing the responses of four separately fabricated electrodes using identical modification and transduction steps. Figure 6(b) displays the statistically derived relative standard deviations (RSDs) at each tested EBVCA-IgA level ranging from 0.1 pM to 10 nM. At higher clinically relevant viral loads, the immunosensor was highly precise with RSDs within 5%. The reproducibility performance was reasonable for measuring moderate virus concentrations down to 0.1 pM. However, lower EBV levels near the LOD produced slightly elevated variability, likely due to the inherent random nature of low analyte binding events.

The selectivity of the electrochemical EBVCA-IgA immunosensor was evaluated by challenging electrodes against other common species in serum that could potentially cause cross-reactive false positive signals. As competing viral agents with clinical relevance, lysozyme, thrombin, glucose oxidase, and hemoglobin were tested at levels of 1 nM. Plotted in Fig. 7(a) are the impedimetric responses after exposing parallel BSPE biosensor electrodes to solutions of the interfering species as well as EBVCA-IgA antigen and blank serum control. The impedance changes (ΔRct) were calculated as:

$$\Delta Rct\ (\%) = (Rct_{sample} - Rct_{blank}) / Rct_{blank} \times 100\%, \quad (1)$$

where Rct_{sample} is the charge transfer resistance measured after incubating the immunosensor with the EBVCA-IgA sample and Rct_{blank} is the baseline resistance of the sensor in blank serum without EBVCA-IgA.

Negligible *Rct* changes of less than 6% were measured after incubating electrodes in lysozyme, thrombin, glucose oxidase, and hemoglobin, which is on par with the blank serum. In contrast, a marked impedance increase of 54% was elicited specifically by the 1 nM EBVCA-IgA, conclusively indicating no sensor cross-reactivity toward the nontarget viruses examined.

Additionally, calibration plots were acquired to compare sensor responses over an extensive concentration range covering low-clinical-relevance loads. As displayed in Fig. 7(b), marginal

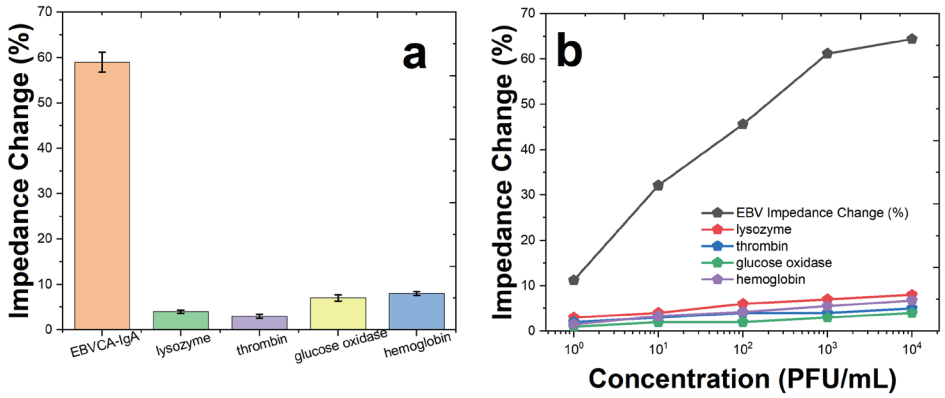

Fig. 7. (Color online) Selectivity assessment showing (a) impedimetric signals and (b) calibration profiles after exposing EBVCA-IgA immunosensor electrodes to 1 nM solutions of lysozyme, thrombin, glucose oxidase and hemoglobin versus EBVCA-IgA.

impedance shifts under 8% *Rct* were observed for the competing molecules even at excessively high 100 nM. The results verify the excellent EBV target selectivity of the developed immunosensing platform against potentially interfering biological media components.

Moreover, we evaluated the selectivity against prevalent nonspecific serum proteins by challenging the immunosensor with high concentrations of human serum albumin (HSA) (50 mg/mL) and human immunoglobulin G (IgG) (10 mg/mL). Negligible *Rct* increases of less than 5% were observed for both HSA and IgG, on par with the blank serum control. The optimized surface blocking evidently prevents nonspecific protein adsorption, ensuring minimal background interference. Collectivity, the selectivity results confirm that the rationally designed EBV immunosensor is capable of resisting false positive responses from both similar viruses and abundant serum proteins, demonstrating suitability for clinical sample analysis.

The analytical performance metrics of the developed EBVCA-IgA immunosensor were benchmarked relative to other reported techniques for viral antibody detection. Most conventional laboratory-based serological assays, including ELISA, immunofluorescence and PCR nucleic acid amplification, impose impractical requirements of lengthy analysis times of more than 2 h, extensive sample handling, and trained personnel. By comparison, the electrochemical immunosensor allows rapid diagnostics within 1 h using minimally processed serum samples. The achievable virus detection limit is more than 100-fold lower than those of lateral flow assays and comparable to those of sophisticated surface plasmon resonance biosensors. Furthermore, the equipment-free disposable sensor lends itself to low-cost manufacturing amenable for decentralized point-of-care viral infection screening.

4. Conclusions

We successfully developed and characterized an ultrasensitive impedimetric immunosensor for the detection of EBVCA-IgA using a biocarbon-based platform, demonstrating significant potential for point-of-care applications. The electrochemical biosensor, utilizing a screen-printed

electrode, exhibited a marked linear detection range from 0.1 pM to 10 nM, with a lower LOD of 33 fM, surpassing the sensitivity of conventional EBV assays. The sensor's robustness was further affirmed by its reproducibility, showing RSDs within 5% at high viral loads, and its exceptional selectivity with negligible cross-reactivity to interference species The rapid response of the sensor, capable of delivering results within one hour, makes it a highly efficient tool for rapid EBV diagnosis. This advancement holds immense promise for clinical and resource-limited settings, offering a pragmatic solution to the challenges posed by current diagnostic techniques, which typically require more than 2 h to produce results and rely on extensive sample processing and laboratory infrastructure. The development of this biosensor represents a significant stride forward in the realm of viral diagnostics and might potentially revolutionize the way EBV is detected and managed in various healthcare contexts.

References

1 H. Y. Hsieh, R. Chang, Y. Y. Huang, P. H. Juan, H. Tahara, K. Y. Lee, D. N. K. Vo, M. H. Tsai, P. K. Wei, H. J. Sheen, and Y. J. Fan: Biosens. Bioelectron. **195** (2022) 113672. https://doi.org/10.1016/j.bios.2021.113672
2 K. Ikuta, Y. Satoh, Y. Hoshikawa and T. Sairenji: Microbes and Infection **2** (2000) 115. https://doi.org/10.1016/S1286-4579(00)00277-X
3 T. Chen, J. Song, H. Liu, H. Zheng, and C. Chen: Sci. Rep. **11** (2021) 10902. https://doi.org/10.1038/s41598-021-90351-y
4 M. A. H. Abusalah, S. H. Gan, M. A. I. Al-Hatamleh, A. A. Irekeola, R. H. Shueb, and C. Yean Yean: Pathogens **9** (2020) 226. https://doi.org/10.3390/pathogens9030226
5 J. Hu, X. Zhang, H. Tao, and Y. Jia: Front. Oncol. **12** (2022) 1034398.
6 J. Xuan, Z. Ji, B. Wang, X. Zeng, R. Chen, Y. He, P. Rao, P. Wu, and G. Shi: Front. Immunol. **11** (2020) 590444.
7 J. E. Gold, R. A. Okyay, W. E. Licht, and D. J. Hurley: Pathogens **10** (2021) 763. https://doi.org/10.3390/pathogens10060763
8 K. Nagata, K. Hayashi, K. Kumata, Y. Satoh, M. Osaki, Y. Nakayama, S. Kuwamoto, Y. Ichihara, T. Okura, and K. Matsuzawa: Endocr. J. (2023) EJ22.
9 R. Rath, P. Kumar, S. Mohanty, and S. K. Nayak: Int. J. Energy Res. **43** (2019) 8931. https://doi.org/10.1002/er.4795
10 Y. Hou, C. C. Lv, Y. L. Guo, X. H. Ma, W. Liu, Y. Jin, B. X. Li, M. Yang, and S. Y. Yao: J. Anal. Test. **6** (2022) 247. https://doi.org/10.1007/s41664-021-00204-w
11 F. Mollarasouli, S. Kurbanoglu, and S. A. Ozkan: Biosensors **9** (2019) 86. https://doi.org/10.3390/bios9030086
12 S. Eissa and M. Zourob: Anal. Chem. **93** (2021) 1826. https://doi.org/10.1021/acs.analchem.0c04719
13 B. Mojsoska, S. Larsen, D. A. Olsen, J. S. Madsen, I. Brandslund, and F. A. Alatraktchi: Sensors **21** (2021) 390. https://doi.org/10.3390/s21020390
14 R. Zumpano, F. Polli, C. D'Agostino, R. Antiochia, G. Favero, and F. Mazzei: Electrochem. **2** (2021) 10. https://doi.org/10.3390/electrochem2010002
15 Z. Zhang, Y. Cong, Y. Huang, and X. Du: Micromachines **10** (2019) 397. https://doi.org/10.3390/mi10060397
16 M. Bandilla, A. Zimdars, S. Neugebauer, M. Motz, W. Schuhmann, and G. Hartwich: Anal. Bioanal. Chem. **398** (2010) 2617. https://doi.org/10.1007/s00216-010-3926-y
17 R. P. A. Balvedi, A. C. H. Castro, J. M. Madurro, and A. G. Brito-Madurro: Int. J. Molecular Sci. **15** (2014) 9051. https://doi.org/10.3390/ijms15059051
18 P. Chen and R. L. McCreery: Anal. Chem. **68** (1996) 3958.
19 P. A. Ferreira, R. Backes, C. A. Martins, C. T. de Carvalho, and R. A. B. da Silva: Electroanalysis **30** (2018) 2233
20 X. Li, J. Zhang, B. Liu, and Z. Su: J. Cleaner Prod. **310** (2021) 127428.
21 X. Gu, Y. Wang, C. Lai, J. Qiu, S. Li, Y. Hou, W. Martens, N. Mahmood, and S. Zhang: Nano Res. **8** (2015) 129.
22 M. Z. M. Mendonça, F. M. de Oliveira, J. M. Petroni, B. G. Lucca, R. A. B. da Silva, V. L. Cardoso, and E. I. de Melo: J. Appl. Electrochem. **53** (2023) 1461.
23 A. Wong, D. G. de Lima, P. A. Ferreira, S. Khan, R. A. B. da Silva, J. L. B. de Faria, and M. Del Pilar Taboada Sotomayor: J. Appl. Electrochem. **51** (2021) 761.
24 A. M. Dehkhoda, N. Ellis, and E. Gyenge: J. Appl. Electrochem. **44** (2014) 141. https://doi.org/10.1007/s10800-013-0616-4

25 S. Kane, A. Storer, W. Xu, C. Ryan, and N. P. Stadie: ACS Sustainable Chem. Eng. **10** (2022) 12226.
26 I. Chakraborty, G. D. Bhowmick, D. Ghosh, B. Dubey, D. Pradhan, and M. Ghangrekar: Sustainable Energy Technol. Assess. **42** (2020) 100808.
27 N. Yadav and S. A. Hashmi: J. Mater. Chem. A **8** (2020) 18266. https://doi.org/10.1039/D0TA06331B
28 M. S. Lashkenari, A. K. Ghasemi, M. Khalid, and S. Shahgaldi: Electrochim. Acta **465** (2023) 142959. https://doi.org/10.1016/j.electacta.2023.142959
29 M. Srivastava, N. R. Nirala, S. Srivastava, and R. Prakash: Sci. Rep. **8** (2018) 1923.